International Journal of Engineering Trends and Technology
ISSN: 2231–5381 / https://doi.org/10.14445/22315381/IJETT-V73I10P124

Volume 73 Issue 10, 312-326, October 2025

Original Article

Deep Learning Based Cardiovascular Disease Detection Using ECG Images

S.G. Bagul[1], S.B. Bagal[2], S.V. Chaudhari[3], B.S. Agarkar[4]

[1,2,3,4]*P.G. Research Centre in Electronics and Telecommunication Engineering, Sanjivani C.O.E, SPPU, Maharashtra, India.*

[1]*Corresponding Author : Sachinbagul1985@gmail.com*

Received: 15 April 2025 Revised: 24 October 2025 Accepted: 28 October 2025 Published: 31 October 2025

Abstract - *Cardiovascular disease is the most significant cause of mortality throughout the globe, as stated by the World Health Organization (WHO). Researchers are interested in detecting Cardiovascular Disease (CVD) using electrocardiography (ECG) images due to their simplicity of use, explainability, visualization, and representational potential. Based on the Deep Learning-Based Two-Way Feature Depiction (DLTWFD), which is derived from a 2-D Deep Convolutional Neural Network (2D DCNN) and a 1-D Deep Convolutional Neural Network (1D-DCNN), this research presents a CVD detection method based on the DLTWFD. For the purpose of providing connection and correlation in the initial ECG pattern, the 2-D DCNN takes the raw ECG pictures as input. To give the correlation between various texture and shape properties of the ECG pictures and to describe the local and global changes in the ECG pattern that are caused by CVD, the 1-D DCNN accepts the Modified Local Ternary Pattern (MLTP) and the Histogram of Oriented Gradient (HOG) features. By combining the deep qualities from raw ECG pictures, texture, and form features of the ECG, the DLTWFD presented improves the uniqueness of the features. The proposed DLTWFD achieves an overall accuracy of 98.20%, a recall of 98.20%, a precision of 98.10%, and an F1-score of 98.05%, surpassing the current state of the art.*

Keywords - *Biomedical Image Processing, Cardiovascular Disease Detection, Deep Convolution Neural Network, Histogram of Oriented Gradients, Local Ternary pattern, Texture Descriptor, Machine Learning.*

1. Introduction

Not only is the heart an essential organ in the body, but it also serves as the driving force behind a person's overall health improvement. The most significant cause of mortality around the globe is cardiovascular disease, which is also referred to as heart disease in certain circles. In 2019, heart disorders were responsible for 32 percent (17.9 million) of all fatalities, according to the WHO. Particularly noteworthy is the fact that heart attacks and strokes were responsible for 85 percent of all deaths [1]. The failure or malfunction of the heart or blood arteries is the primary causal factor in the development of cardiac disorders. Nearly three-quarters of all fatalities that are caused by heart illnesses take place in nations that have incomes that fall between the middle and poor levels [2]. Heart disease is the most significant cause of death among all illnesses that do not result from an infectious agent. Behavioral factors, such as a poor diet, smoking, tobacco use, weight, excessive alcohol consumption, excessive salt consumption, and a lack of physical activity, as well as physiological factors, such as high blood pressure, cholesterol, high glucose, and high blood sugar, are significant contributors to the development of heart diseases [3, 4]. Pain or discomfort in the chest, arm, elbow, left shoulder, back, or jaw, unconsciousness, trouble balancing, sudden vision loss, difficulty speaking, cold sweats, dizziness, a severe headache, or difficulty speaking are some of the symptoms that most commonly accompany cardiac issues. Other symptoms include speech difficulties, cold sweats, dizziness, and sudden loss of vision. These groupings may include a variety of heart problems, including but not limited to heart failure, coronary heart disease, stroke, peripheral artery disease, venous disease, subclinical atherosclerosis, congenital heart disease, peripheral heart disease, valve disease, and other heart illnesses [5, 6]. Both non-surgical and surgical methods are also used in the process of diagnosing heart problems. Invasive procedures include coronary angiography and blood testing, to name just two examples. The ECG, Coronary Computed Tomography Angiograms (CCTA), cardiac Magnetic Resonance Imaging (MRI), and echocardiograms are all examples of non-invasive procedures. Electrocardiograms are among the numerous non-invasive, low-cost, and straightforward procedures used to diagnose heart disease. Therefore, electrocardiograms have become the method of choice for identifying and diagnosing cardiac diseases, such as myocardial infarction, arrhythmia, pericarditis, electrolyte imbalances, and pulmonary illnesses [7-9]. This has led to the widespread acceptance of electrocardiograms as the preferred technique.

The overall framework of a machine learning-based Electrocardiogram (ECG)- based cardiovascular disease detection system is illustrated in Figure 1. The classification system incorporates a wide range of processes, including signal pre-processing, feature extraction, feature selection, classification, and the identification of heart disease. The technology can diagnose cardiac problems by using either an ECG signal or an image. The input signal is often contaminated with noise and artifacts due to the presence of internal body components and electrode connections.

Motion artifacts, wandering baseline artifacts, loose lead artifacts, muscle tremor artifacts, arterial pulse trapping artifacts, echo distortion artifacts, neuro-modulation artifacts, electromagnetic interference, and other similar artifacts are some of the key artifacts that may be seen on an ECG. Normalization, noise reduction, cropping, and artifact rejection are some of the additional steps included in the pre-processing stages of electrocardiogram records. Capturing the features of the ECG signal is a crucial component of the feature extraction process [10]. These features represent the changes in the signal that are brought about by abnormalities. An ECG signal may be used to extract a wide variety of parameters, including morphological and derived characteristics. Morphological characteristics, including the length of the QRS complex, the duration of the P wave, the ST segment, the PR interval, the Q wave valley, the T wave valley, and other components, distinguish the pattern of the heartbeat. A number of these characteristics are also included. [11] Some of the characteristics that were developed include the Discrete Wavelet Transform (DWT), the Zero Crossing Rate (ZCR), the Principal Component Analysis (PCA), the Independent Component Analysis (ICA), the Empirical Mode Decomposition (EMD), the Vector Cardiography (VCG) vector, eigenvectors, and other similar features. For machine learning, feature extraction is a vital component since it enables the collection of the EEG signal's most essential and distinguishing characteristics.

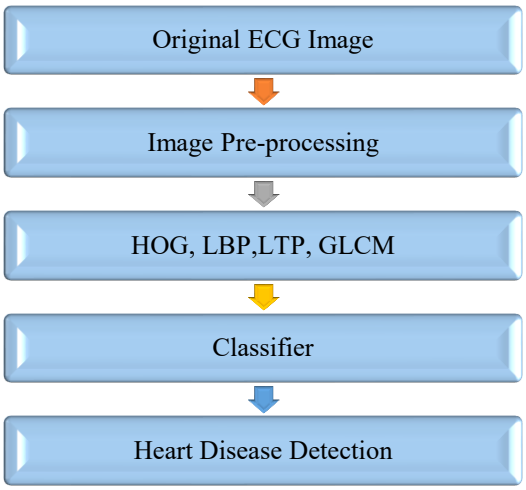

Fig. 1 Generalized framework of CVD system

In the field of CVD, some of the imaging modalities that are used include Computed Tomography (CT), Single Photon Emission Computed Tomography (SPECT), MRI, and echo imaging. Different approaches have been taken to CVD based on its form, texture, and severity. Machine learning-based algorithms that utilize the features of texture, form, or color may be employed to screen medical images for anomalies [12, 13].

Various ML and DL-based CVD detection techniques have been presented in recent decades, which focus on the ECG signal. However, these techniques provide poor results due to poor spatial correlation, lower interpretation capability of models, higher complexity of DL models, class imbalance problem, and less standardization in the CVD detection scheme. Significantly less concentration is given to CVD detection using images that provide a texture depiction of the ECG pattern. Therefore, it is essential to focus on improving the accuracy of CVD detection using an effective complex pattern feature representation of the ECG images.

In this study, the DLTWFD for CVD is presented based on ECG images to enhance the accuracy of CVD identification. This article makes several significant contributions, which are summarized as follows:

- The 2-D DCNN) DLTWFD uses the 1-DCNN to enhance the feature representation of ECG images. If you want to portray aberrant patterns in ECG pictures, the 2-D DCNN provides greater spatial connectivity and correlation of the raw ECG images. A correlation in the textural and form qualities of the ECG pictures is provided by the 1-D DCNN, which utilizes innovative MLTP and HOG features.
- Using accuracy, precision, recall, and F1-score, the performance assessment of the suggested CVD detection technique is being carried out.

Continuing, the remainder of the article is organized as follows: Section 2 discusses the work relevant to identifying cardiovascular disease using electrocardiograms. Within the third section, comprehensive mathematical modeling, formulation, and approach are presented. The fourth section provides a concise summary of the experiment's outcomes, along with additional remarks. Lastly, the findings and potential future applications of the CVD detection system are presented in Section 5.

2. Related Work

ECG pictures have seen a significant increase in their use for the identification of CVD due to their visual interpretability and ease of use. Over the past decade, machine learning has become the most widely used method for diagnosing heart disease. The HRV signal was decomposed into its subbands by Giri et al. [19], who utilized the Discrete Wavelet Transform (DWT) for this purpose. The use of PCA,

ICA, and LDA achieved a reduction in the dimensionality of the sub-band DWT coefficients. An accuracy of classification of 96.8% was achieved using the ICA and Gaussian mixture model. During the process of HRV signal decomposition, Patidar et al. [20] investigated tunable-Q wavelet transform sub-bands using Principal Component Analysis (PCA) for feature reduction and centered correntropy for feature calculation techniques. The accuracy of the LSSVM classifier was 99.72%. HRV signals are broken down using the FAWT analytical wavelet transform [21] developed by Kumar et al.

We discovered that it is possible to derive nonlinear entropy-based features from sub-band data. They achieved a perfect score in the Coronary Artery Detection (CAD) test using their approach. Sood and his colleagues described an Empirical Mode Decomposition (EMD) for HRV intrinsic mode functions in a publication [22]. With p-values lower than 0.05, the most discriminative features for CAD were the mean frequency characteristics calculated from the Fourier-Bessel expansion, the amplitude modulation bandwidth, and the frequency modulation bandwidth. An SVM-based Coronary Artery Disease (CAD) detection system was developed by Alizadehsani et al. [23] to recognize CAD and diagnose heart ailments. An Artificial Neural Network (ANN) model was developed by Arabasadi et al. [24] using a Multilayer Perceptron (MLP) structure with a sigmoid exponential function. This was accomplished by using four well-known ranking algorithms to select more essential traits.

To develop the ANN model, the genetic approach begins by accurately detecting Coronary Artery Disease (CAD) with a 93.85% accuracy rate. A description of SVM-based CVD detection may be found in Tabassum and Islam [25]. The percentage of patients who had apnea, sinus tachycardia, atrial fibrillation, and myocardial infarction was determined to be 84.6%. The SVM was trained using the following parameters: the RR interval, the QRS complex, the ST elevation, the heart rate, the ST interval, and the PR interval. In their study [26], Gauvane and colleagues presented an MLP-based approach for detecting heart disease. This algorithm is trained using data from various factors, including physical characteristics, blood pressure, cholesterol levels, and blood sugar levels. The accuracy of this solution is 0.91, and its recall is 0.89. The Hybrid Recurrent Function with Linear Model (HRFLM) was used by Mohan et al. [27] to diagnose cardiac disease with an accuracy rate of 88.7% in the Cleveland dataset. The selection of efficient features limits the system's performance.

Following that, Sharma et al. [28] demonstrated the diagnosis of cardiac disease using KNN, SVM, NB, and DNN. The SVM algorithm yields results superior to those obtained by DNN (81.9%), NB (83.97%), and KNN (81.43%) when applied to the Pittsburgh dataset. There is a possibility that the system's efficiency and efficacy might be improved by employing generative models to produce a synthetic dataset. The authors Li et al. [29] proposed a feature selection technique based on conditional mutual information, which is an efficient approach. FCMIM-SVM achieved an accuracy of 92.37% when used on the Cleveland dataset for the detection of heart disease. The FCMIM expedited processing by prioritizing the most critical information. The outcomes of machine learning-based techniques are highly dependent on the quality, uniqueness, and number of features. Several different classifiers for Cardiovascular Disease (CVD) were created by Prajwal et al. [30], including SVM, KNN, GB, ANN, and HV. The accuracy rates are 72.68% for SVM, 70.03% for GB, 71.32% for HV, 66.14% for KNN, and 72.51% for ANN. They developed features based on body mass index I), which assist in identifying.

Using ECG data, Fang et al. [31] proposed the use of RBF-SVM for the purpose of identifying cardiac disease. The Pan-Tompkins and K-means clustering algorithms were used to extract and select QRS characteristics. A total accuracy of 98.98% was achieved. When compared to standard samples, which had an accuracy rate of 99.74%, aberrant samples had a lower accuracy rate of 97.53%. A study conducted by Biswas et al. [32] investigated the impact that feature selection strategies had on SVM, RF, LR, KNN, NB, and DT machine learning classifiers. Mutual information, analysis of variance, and chi-square were used. The RF + MuI classifier achieves a success rate of 94.51%, surpassing the accuracy of other feature options. Based on the comprehensive review of the existing literature, the following research gaps have been identified:

- Inadequate spatial correlation and textural portrayal
- The number of ECG images reduces the efficiency of CVD identification [33, 34].
- The issue of class imbalance and data scarcity arises as a result of unequal training and a shortage of public ECG images used for training deep learning models [35, 36].
- Low levels of both explainability and interpretability of the algorithm [38, 39]. Baseline drift, motion artifacts, and power line interference all contributed to the system's poor performance.
- Less work is done on CVD detection using images that provide a texture depiction of the ECG pattern.
- Lower accuracy for multiclass CVD detection
- Lower “Explainability and Interpretability” in the ECG signal-based CVD detection
- Complexity in the existing techniques is due to higher training parameters and the intricacy of the model framework.
- Lower spatial correlation in the complex ECG patterns.

3. Methodology

The suggested DLTWFD-based CVD detection technique is shown diagrammatically in Figure 2, available here. Initially, the ECG photos are preprocessed to crop the header and footer of the images. This cropping does not

represent any information about the ECG or health condition of the individual. Two deep convolutional neural network arms make up the FLTWFR. These arms mix raw pictures with morphological, form, and textural characteristics. To learn the hierarchical characteristics of the ECG from two-dimensional images, a Two-Dimensional Deep Convolutional Neural Network (2D-DCNN) is employed. Providing the connection between the form, texture, and morphological characteristics of the ECG, the second arm comprises a one-dimensional DCNN capable of accepting numerous ECG features. These features include HOG-based shape features, MLTP-based texture features, and morphological aspects of the ECG. A flattening and concatenation process is performed on the features of the final layers of both the 2D-DCNN and the 1D-DCNN representations. To improve the connection between neurons, the concatenated characteristics are sent to the FC layer. In conclusion, a softmax classifier is used to categorize ECG images into the following categories: Abnormal Heartbeat (AH), Myocardial Infarction (MI), History of Myocardial Infarction (HMI), and normal.

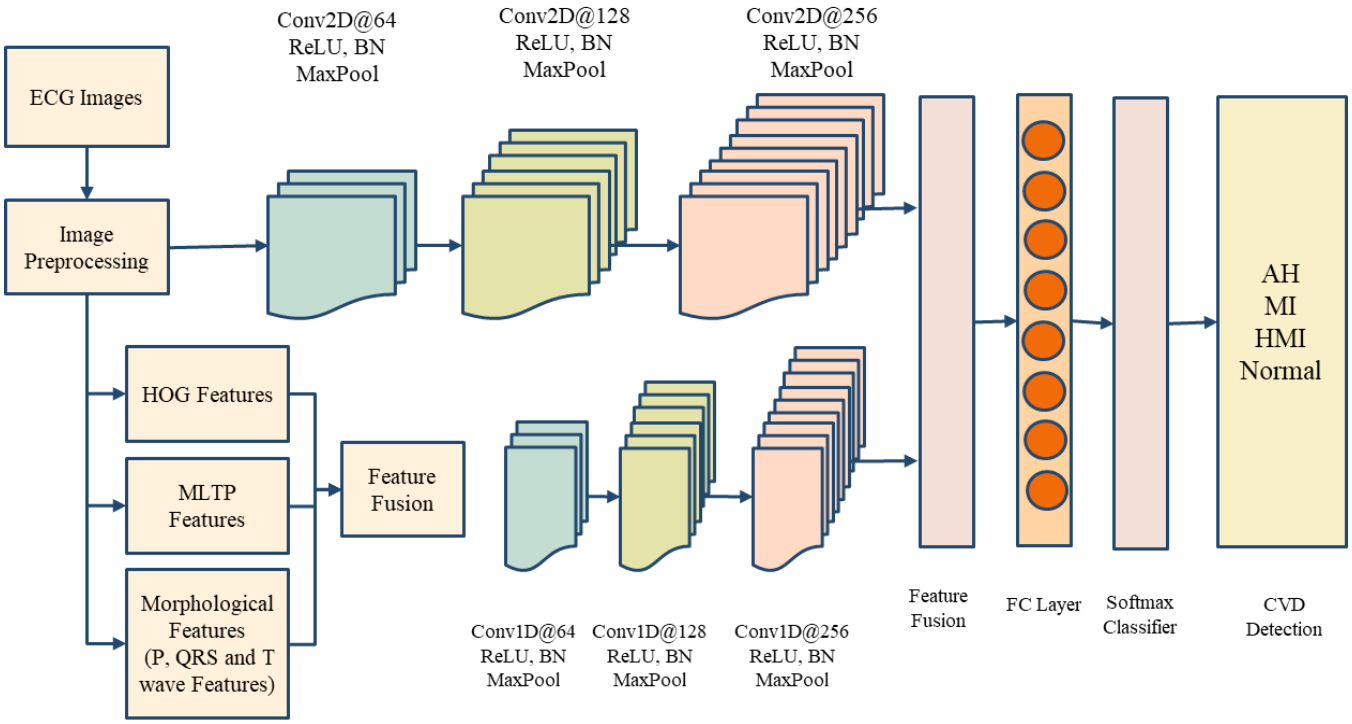

Fig. 2 Flow diagram of the proposed DLTWFD-based CVD detection scheme

To establish spatial connections in the ECG images, the first arm comprises a three-layered, two-dimensional DCNN. Following the Rectified Linear Unit (ReLU) layer, the Batch Normalization layer (BN), and the maximum pooling (MaxPool) layer, the two-dimensional DCNN is composed of three convolutional layers, each with 64, 128, and 256 filters of varying sizes. Within the ECG pattern, the convolution layer provides correlation and connection to portray the changes caused by illnesses.

The convolution process of a two-dimensional Deep Convolutional Neural Network (DCNN) for ECG images, with a resolution of Row × Col and a filter kernel W, is represented by Equation 1. When it comes to the Conv layer, filters that have dimensions of 3×3 and a stride of 1 pixel are used. It is generally accepted that the initial settings of the Conv filters are set arbitrarily.

$$Conv(x,y) = \sum_{i=1}^{Row} \sum_{j=1}^{Col} ECG(i-x, j-y) W(x,y) \qquad (1)$$

In accordance with equation 2, the ReLU layer contributes to the enhancement of the non-linear character of the output of the convolution layer by converting all negative neurons to zero. Through the use of the ReLU layer, training performance is improved, and training is accelerated.

$$\text{Relu}(x,y) = \max(0, \text{conv}(x,y)) \qquad (2)$$

The MaxPool layer is responsible for selecting the most valuable values from the local 2×2 pixel area to reduce the number of features and eliminate redundant ones. By taking into account the mean (m) and standard deviation of neurons throughout the batch size of 32, as well as two trainable parameters—scale (α) and offset (γ) —which are initialized randomly, the BN layer can normalize the output of the ReLU layer. In the case of the 2D DCNN, the BN operation may be expressed as equation 3.

$$\text{BN}(x,y) = \alpha . \frac{ReLU(x,y) - m}{\sigma} + \gamma \qquad (3)$$

To provide connection and correlation between local and global textural, MLTP, and morphological characteristics of ECG, the second arm comprises a one-dimensional DCNN. There are also three layers of one-dimensional convolution in the one-dimensional DCNN, with 64, 128, and 256 filters at each layer, followed by layers of ReLU, BN, and MaxPool. Following the flattening of the output of the MaxPool layer in the 2-D DCNN and the 1-D DCNN, a 1-D vector is then sent to the Fully Connected Layer (FCL), which has fifty hidden layers. Through the process of merging each deep feature with all of the other characteristics, the FCL can improve the connectedness between profound features. The probabilistic softmax classifier is also applied to categorize the electrocardiogram images into the following categories: AH, HMI, MI, and normal.

3.1. MLTP Features

When compared to the two levels of banalization included in LBP, the LTP is an upgraded form of LBP that considers three additional levels. The LTP provides superior local spatial features, which can reflect the changes that occur locally in the pictures. By dividing the picture into local patches of 3×3 pixels, the LTP technique is used. This is the value that is deemed to be the threshold. A comparison is made between the values of the nearby pixels and the value of the Centered Pixel (CX), and if the value is greater than CX +th, then the pattern is judged to be 1. If the value of the surrounding pixel is lower than the CX-th, the pattern is regarded as having a value of -1. According to equation 4, the pattern is deemed to be identical to zero if the value of the adjoining pixel falls within the range of CX+th to CX-th.

$$ltp(x) = \begin{cases} -1 & if\ x < CX - th \\ 0 & X - th \le x \le CX + th \\ 1 & if\ x > CX + th \end{cases} \quad (4)$$

The L-LTP is produced by changing 1 to 0 and -1 to 1, thereby generating a binary pattern. The U-LTP is constructed by changing -1 to 0, while the L-LTP is constructed by changing 1 to 0. After being translated to a decimal equivalent, the binary sequence of L-LTP and U-LTP yields a result that falls anywhere between 0 and 255. This is because there are eight neighbors.

The threshold value, which is manually determined, has a significant impact on the results when the LTP is examined. Additionally, the LTP characteristics can be affected by noise as well as uneven fluctuations in light throughout the image. For the purpose of assessing the correlation, the standard LTP considers a single neighbor, which is susceptible to being influenced by noise and uneven contrast.

3.2. Modified LTP Features

When evaluating textures, the standard LTP only considers close neighbors, which reduces its resilience when dealing with noisy or low-contrast images. A further disadvantage of typical LTP is its weak spatial connectivity, which reduces classification ability. Multiple neighbors, with a maximum of three layers, are considered for the assessment of texture in the unique Modified LTP (MLTP) that has been developed. The MLTP considers eight neighbors, and cap C sub, 1 minus 8 end subscript are located at the corresponding radii R1=1, R2=2, and R3=3.

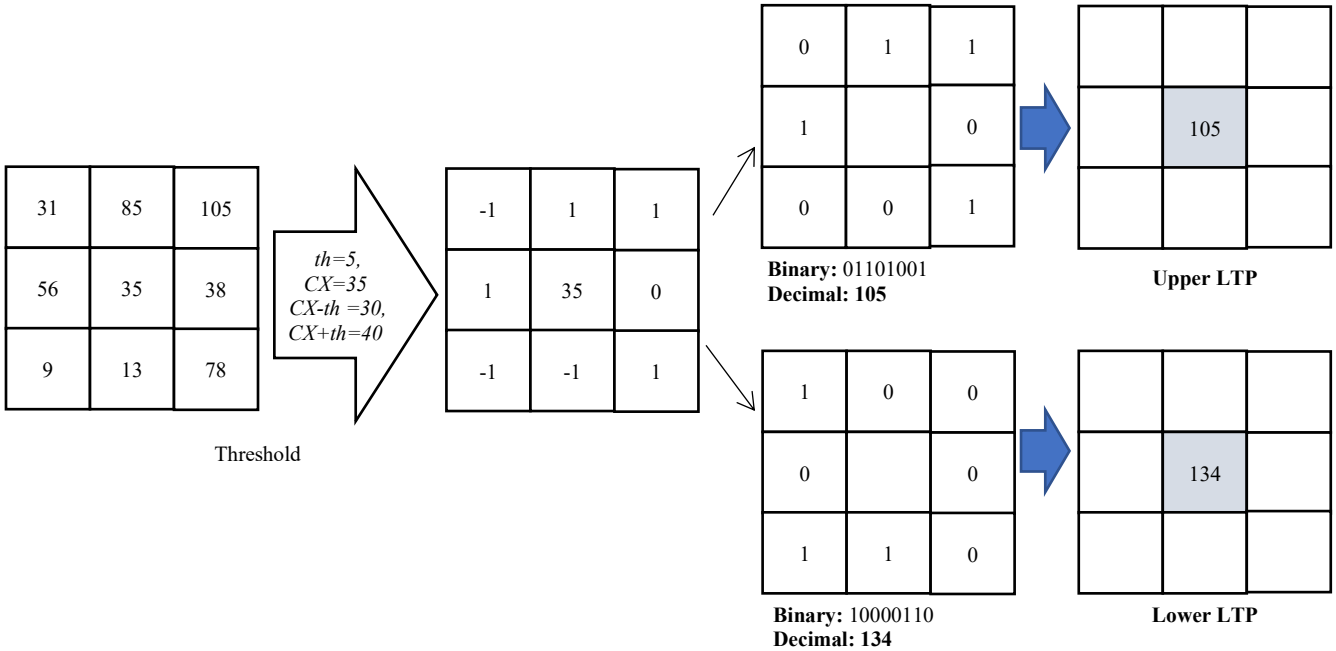

Fig. 3 Visualization of the LTP process

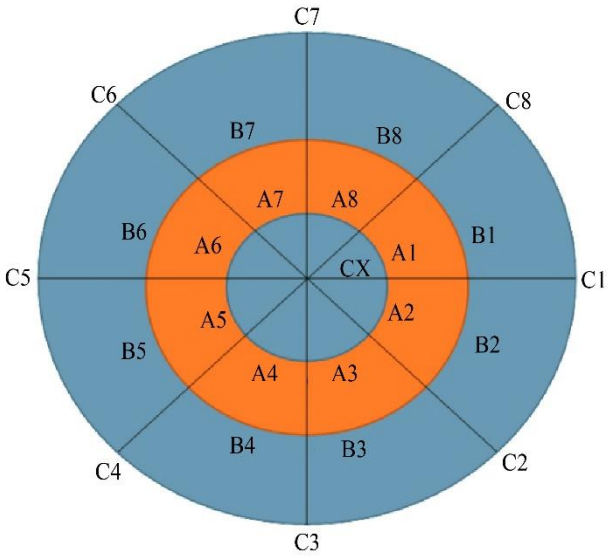

Fig. 4 Spatial representation of MLTP

MLTP provides the connection between the center pixel and its three adjacent pixels to achieve a more accurate depiction of the texture.

Using Equation 3, which assigns a larger weight to the immediate neighbor than the neighbor at radius R3=3, the equal surrounding pixel value is taken into consideration. Figure 5 illustrates the procedure involved in MLTP.

$$x = (A_i - CX) \times R3 + (B_i - CX) \times R2 + (C_i - CX) \times R1 \quad (5)$$

Following the division of the ULTP and LLTP into the N×N blocks, the histograms of each block are individually calculated. To construct the final feature vector, the histograms from each block are concatenated. When the picture is divided into blocks, it becomes easier to capture the fluctuations in the electrocardiogram signals present in the local area. The single-block characteristics are inadequate in comparison to the spatial connection offered by this. There are 512 features available in the MLTP histogram single block (N = 1), with 256 features for ULTP and 256 features for LLTP.

These features are designed to provide scale and shift invariance. When the value of N is equal to two, the LLTP and ULTP descriptors are separated into equal blocks of 2×2 local regions. Each of these blocks is composed of a total of (row/2) rows and (cols/2) columns, where row and col represent the number of rows and columns initially present in the picture. Table 1 provides a summary of the MLTP feature vector dimensions for each block. Figure 6 presents a visual representation of the MLTP properties, along with the corresponding histogram.

Table 1. MNLTP features for different blocks

Number of Blocks (N)	ULTP Features (Histogram values)	LLTP Features (Histogram values)	Total Features
N=1	256	256	512
N=2	1024	1024	2048
N=3	2304	2304	4608
N=4	4096	4096	8192
N=5	6400	6400	12800

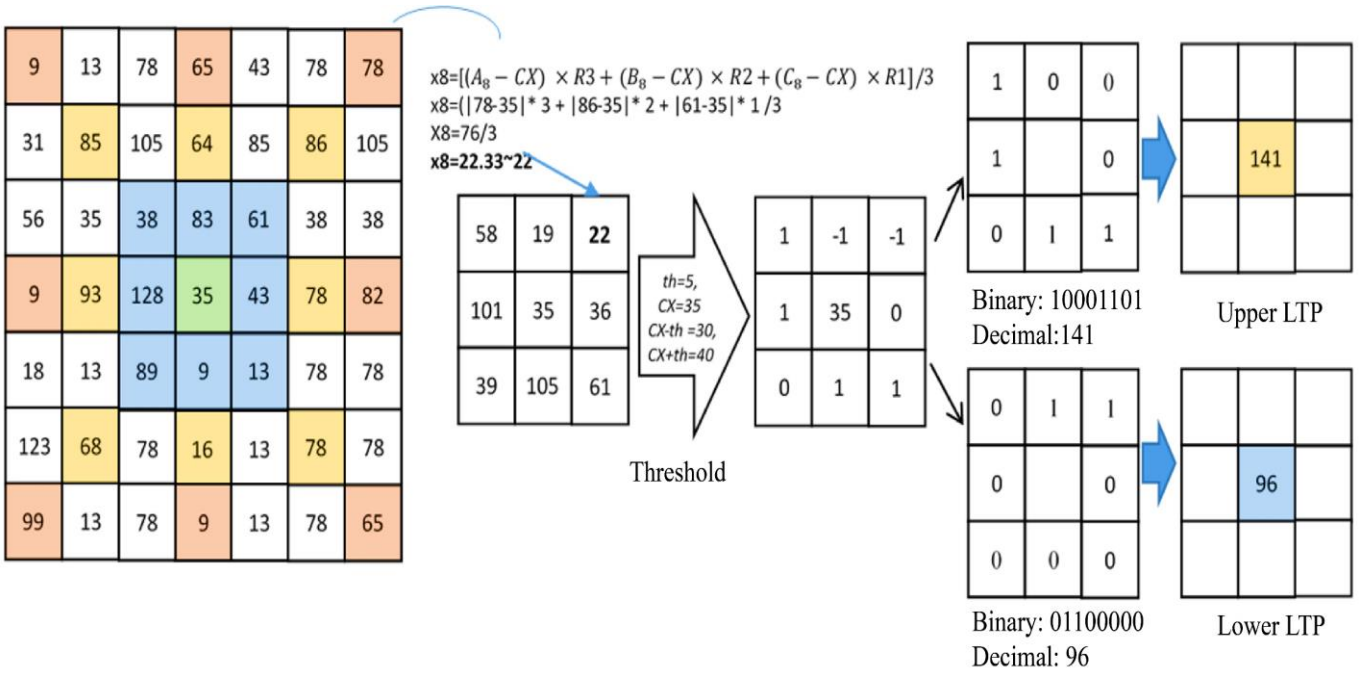

Fig. 5 Process of MLTP

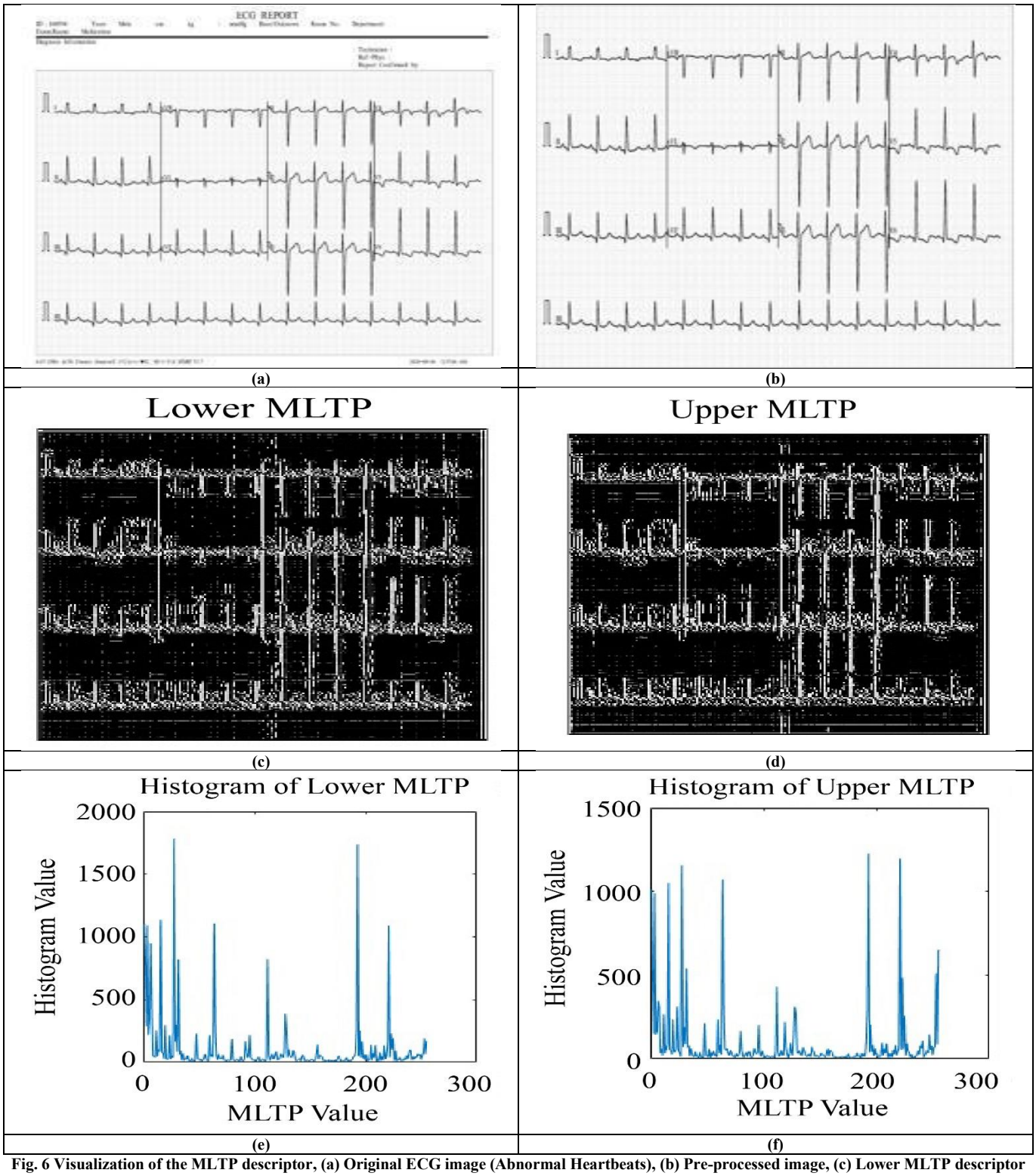

Fig. 6 Visualization of the MLTP descriptor, (a) Original ECG image (Abnormal Heartbeats), (b) Pre-processed image, (c) Lower MLTP descriptor (d) Upper MLTP descriptor, (e) Histogram of lower MLTP, and (f) Histogram of upper MLTP.

3.3. HOG Features

It is possible to define the form of objects present in remote sensing photos by using the HOG, which provides the orientation of gradients in various directions. The computation of the horizontal (Ix) and vertical (Iy) gradients is accomplished by using a horizontal derivative filter (Hx) and a vertical derivative filter (Hy) with equations 6-9, respectively.

$$Hx = [-101] \quad (6)$$

$$Hy = [-101]^T \quad (7)$$

The magnitude of the orientation gradient, denoted as M, is determined by using the value of 10. In contrast, the orientation, denoted as θ, is computed considering nine bins ranging from 0 to 180 degrees.

The total concentration of the edges is determined by the magnitude and direction, which is used to define the anomalies in the ECG structure.

$$Ix = im * Hx \quad (8)$$

$$Iy = im * Hy \quad (9)$$

$$M = \sqrt{Ix^2 + Iy^2} \quad (10)$$

$$\theta = tan^{-1}\left(\frac{Iy}{Ix}\right) \quad (11)$$

Initially, the pictures are normalized using the second normalization form to address the issue of changes in lighting. The picture is divided into local blocks, each composed of 2×2 cells with a size of 8×8 pixels. For the purpose of enhancing contrast, the blocks are deemed to overlap by fifty percent.

The computation of nine bin histogram features for each cell yields a total of 34,596 features for an image of size 256×256. The HOG visualizations are shown in Figure 7, which includes horizontal gradients (Figure 7(a)), vertical gradients (Figure 7(b)), and the magnitude of gradients (Figure 7(c)), respectively.

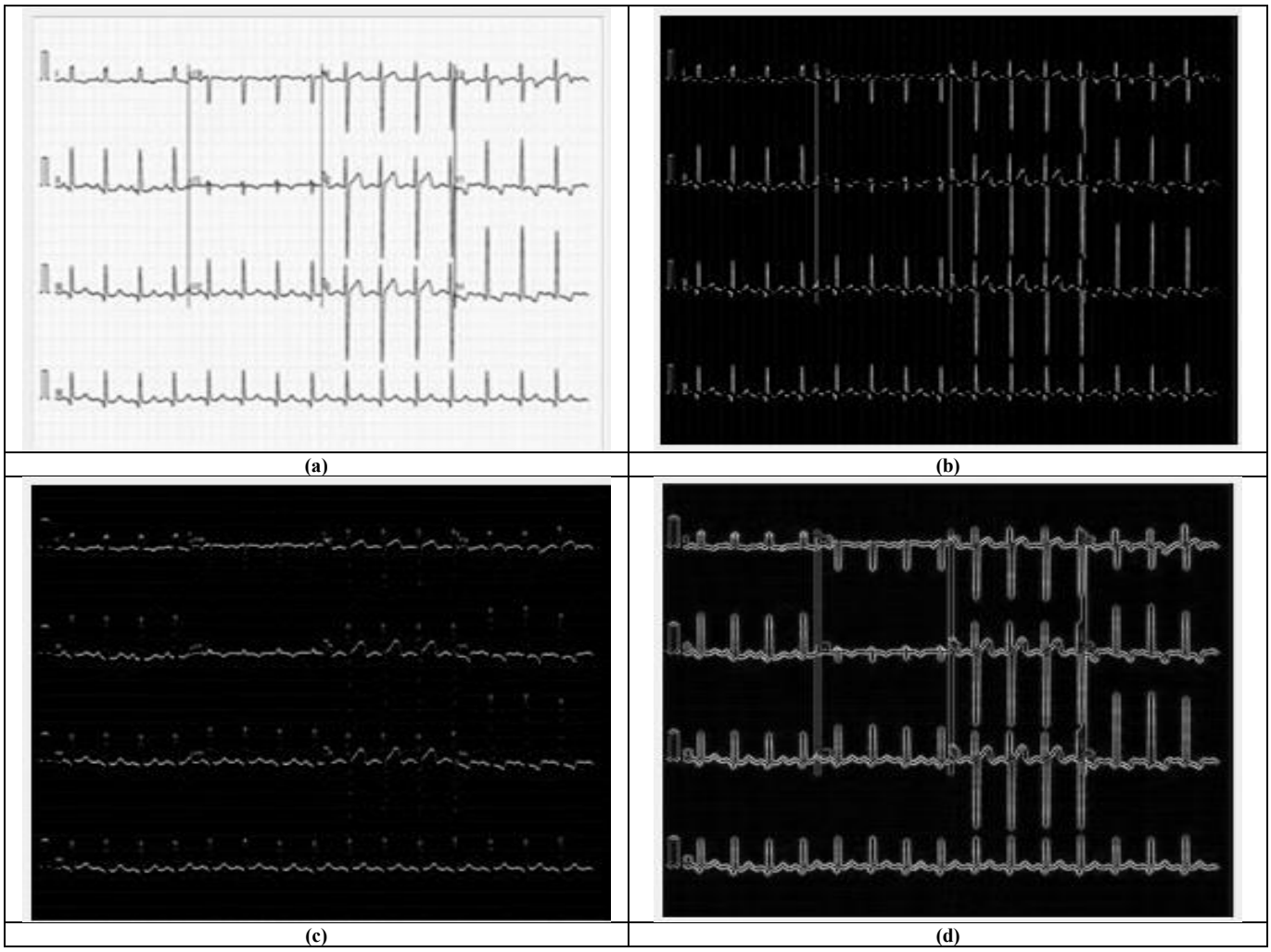

Fig. 7 Visualization of HOG (a) Preprocessed ECG image, (b) Horizontal gradient, (c) Vertical gradients, and (d) Magnitude of HOG.

3.4. Morphological Features

An improvement in signal quality is achieved by using preprocessing methods, such as filtering and normalization, to extract P, QRS, and T morphological characteristics from ECG images. Waveform boundaries can be identified using edge detection techniques, such as the Canny or Sobel filters.

Wavelet transformations and adaptive thresholding are two examples of segmentation methods that may be used to specifically separate the P wave, QRS complex, and T wave. Approaches of feature extraction include peak identification, amplitude measurement, and duration computation. These approaches quantify essential characteristics, such as the duration of the P-wave, the breadth of the QRS complex, and the shape of the T-wave. The morphological characteristics consist of three P-wave features, which include duration, amplitude, and area of the P-wave; five QRS wave features, which include QRS length, R-wave amplitude, Q-wave amplitude, S-wave amplitude, and QRS area; and three T-wave features, which include duration, amplitude, and area of the T-wave. To optimize the feature representation, the final feature vector comprises 8192 MLTP features, 34596 features, and 11 morphological characteristics. These features are then input into a 1-D deep convolutional neural network.

4. Experimental Results and Discussion

On a personal computer with 16 gigabytes of Random-Access Memory (RAM) and Windows as the operating system, the suggested solution utilizes MATLAB 2024. A batch size of 32 and an initial learning rate of 0.001 are considered during the training of the proposed algorithm, which is trained using the Adam optimization method for a total of 200 epochs. As shown in Figure 8, the model achieves a training accuracy of 100% for the entire 200 epochs and demonstrates stability in training beyond the 100th epoch. Table 2 provides a summary of the hyperparameters that are used during training.

Table 2. Hyperparameters of DCNN

Parameter	Specification
Learning Algorithm	Adam
Batch Size	32
Initial Learning Rate	0.001
Loss Function	Cross-Entropy
Activation Function	ReLU
Epoch	200

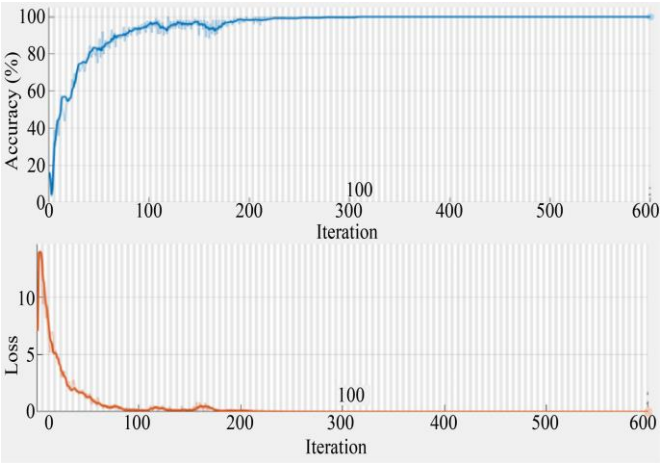

Fig. 8 Training performance of DLTWFD

4.1. Dataset

Among the pictures that comprise the public Mendeley ECG image collection [33], four categories are employed for performance assessment. These categories include Myocardial Infarction (MI), History of Myocardial Infarction (HMI), and normal and Abnormal Heartbeat (AH). Each ECG contains four ECG signals for the patient.

There are 233 photographs of AH, 239 images of MI, 172 images of HMI, and 284 images of normal that are included in the collection. A resolution of 2213×1572 pixels is available for the ECG pictures.

The material in the footer and header that does not represent any information related to ECG is clipped during the pre-processing stage of the software development process. Seventy percent of the dataset is used for training CVD, while thirty percent is used for testing CVD.

4.2. Discussions on Results for the 4 Class CVD Detection

Additionally, the confusion matrix for the raw pictures plus 2-DCNN, ECG features plus 1-D DCNN, and DLTWFD is shown in Figures 9-11, respectively. Following the implementation of the DLTWFD, the four-class CVD detection achieved an exceptional overall accuracy of 98.20%, a recall of 98.20%, a precision of 98.10%, and an F1-score of 98.05%.

For the diagnosis of four-class cardiovascular disease, the 2D-DCNN has an average recall of 94.58%, precision of 94.83%, F1-score of 94.66%, and accuracy of 94.58%. On the other hand, the results of the four-class CVD detection using 1D-DCNN were as follows: an overall recall of 96.68%, a precision of 96.75%, an F1-score of 96.70%, and an accuracy of 96.68%.

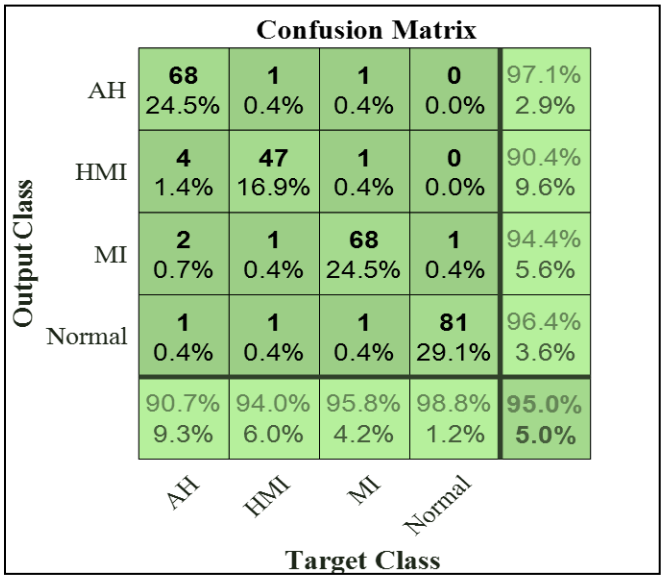

Fig. 9 Confusion matrix for 2-D DCNN-based CVD detection

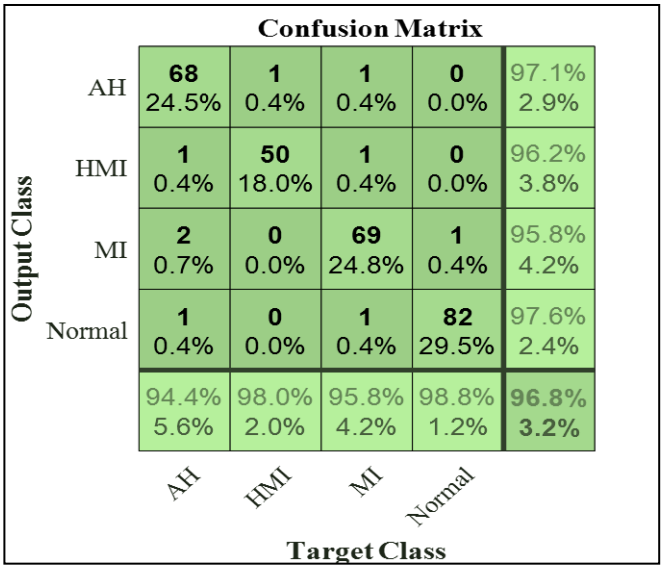

Fig. 10 Confusion matrix for 1-D DCNN-based CVD detection

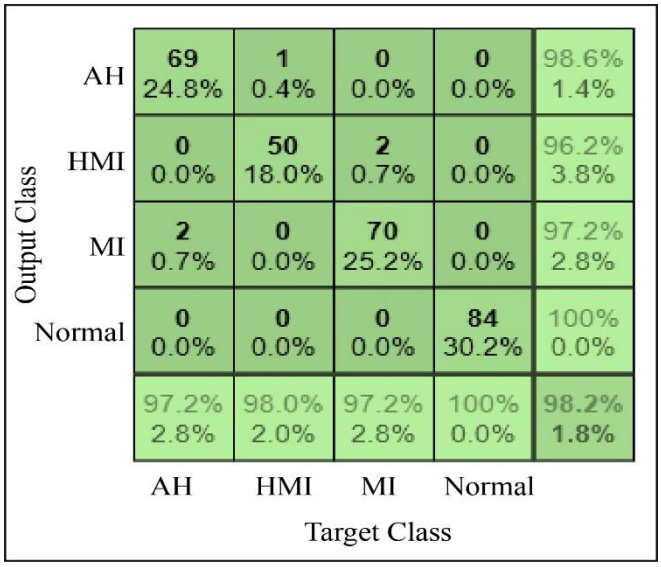

Fig. 11 Confusion matrix for DLTWFD-based CVD detection

A greater accuracy of 98.2% is provided by the DLTWFD in comparison to the 2-D DCNN (94.58%) and the 1-D DCNN (98.68%). This precision is achieved by integrating the benefits of raw pictures with the texture, form, and morphological characteristics of the electrocardiograms. In terms of overall recall, the DLTWFD offers 100% recall for the normal, 96.20% for the HMI, 97.2% for the MI, and 98.60% for the AH. With a precision of 100% for normal, 98% for HMI, 97.20% for AH, and 97.2% for MI, the DLTWFD will give them accurate results. The F1-Scores for the DLTFWR are 97.1%, 98.1%, 97.2%, and 100%, respectively, for the AH, HMI, MI, and regular classes. While the DLTWFD has a greater accuracy for the normal (100%) and a lower accuracy for the HMI (96.20%), the normal has superior accuracy. The DLTWFD contributes to the enhancement of the spatial correlation and connection in the local, global, and morphological characteristics of the ECG. A 2-D DCNN using raw images and a 1-D DCNN with various characteristics demonstrate the imbalance between recall and accuracy.

Figure 10 presents graphics that demonstrate the visualizations of the data obtained by the DLTWFD.

Table 3. Comparative results of CVD detection using DLTWFD

Perfor-mance Parameter	Method	AH	HMI	MI	Normal	Average
Recall	2-D DCNN	97.1	90.4	94.4	96.4	94.58
	1-D DCNN	97.1	96.2	95.8	97.6	96.68
	DLTWFD	98.6	96.2	97.2	100	**98.2**
Precision	2-D DCNN	90.7	94	95.8	98.8	94.83
	1-D DCNN	94.4	98	95.8	98.8	96.75
	DLTWFD	97.2	98	97.2	100	**98.1**
F1-score	2-D DCNN	93.79	92.16	95.09	97.59	94.66
	1-D DCNN	95.73	97.09	95.8	98.2	96.7
	DLTWFD	97.89	97.09	97.2	100	**98.05**
Accuracy	2-D DCNN	97.1	90.4	94.4	96.4	94.58
	1-D DCNN	97.1	96.2	95.8	97.6	96.68
	DLTWFD	98.6	96.2	97.2	100	**98.2**

4.3 Discussions on Results for 2-Class CVD Detection

The performance of the DLTWFD is evaluated for two-class classification, considering one regular class versus one sick class and one illness versus another disease, as shown in Figures 12 and 13. In terms of overall accuracy, the DLTWFD achieves scores of 98.55 percent for AH versus Normal, 99.05 percent for HMI versus Normal, 100 percent for MI versus Normal, 98.35 percent for AH versus HMI, 99.05 percent for HMI versus MI, and 98.6 percent for AH versus MI, respectively. When the findings are compared with those of a typical class, DLTWFD achieves a classification accuracy of 100% for MI, surpassing the conventional classification. The two-class disease detection demonstrates a higher F1-score, with values of 98.70% for AH vs. Normal, 99.22% for HMI vs. Normal, 100% for MI vs. Normal, 98.35% for AH vs. HMI, 99.17% for HMI vs. MI, and 98.60% for AH vs. MI, respectively. As shown in Table 4, the outcomes of the DLTWFD are evaluated for the various block sizes that are

used in the MLTP. The MLTP yields higher-quality results for the radius R = 3 and four blocks (N = 4) than any other method. For a sample size of four, the DLTWFD provides an accuracy of 89.93% for R=1, 94.58% for R=2, 98.20% for R=3, 97.46% for R=4, and 96.36% for R=5. When the radius is increased, the spatial correlation also increases, and the homogeneity measure of the texture is provided up to R = 3. However, when the radius is increased beyond R = 3 (i.e., R = 4 and R = 5), the spatial correlation is low, and it fails to achieve spatial homogeneity.

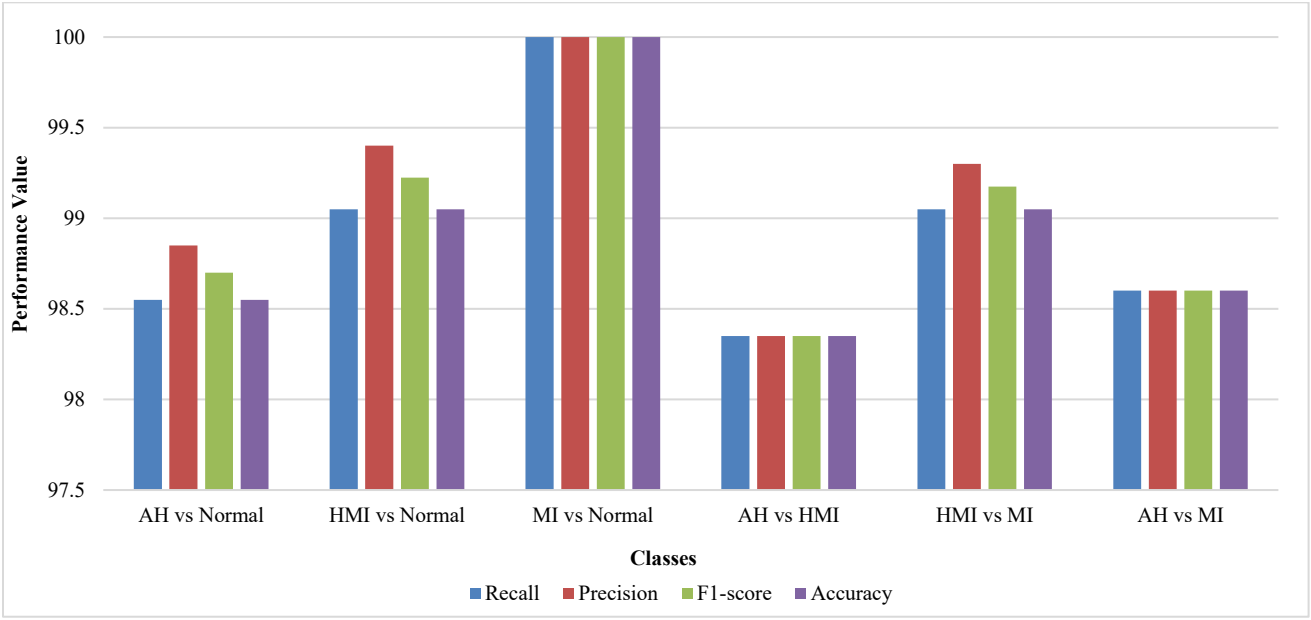

Fig. 12 Performance of the DLTWFD for two-class classification

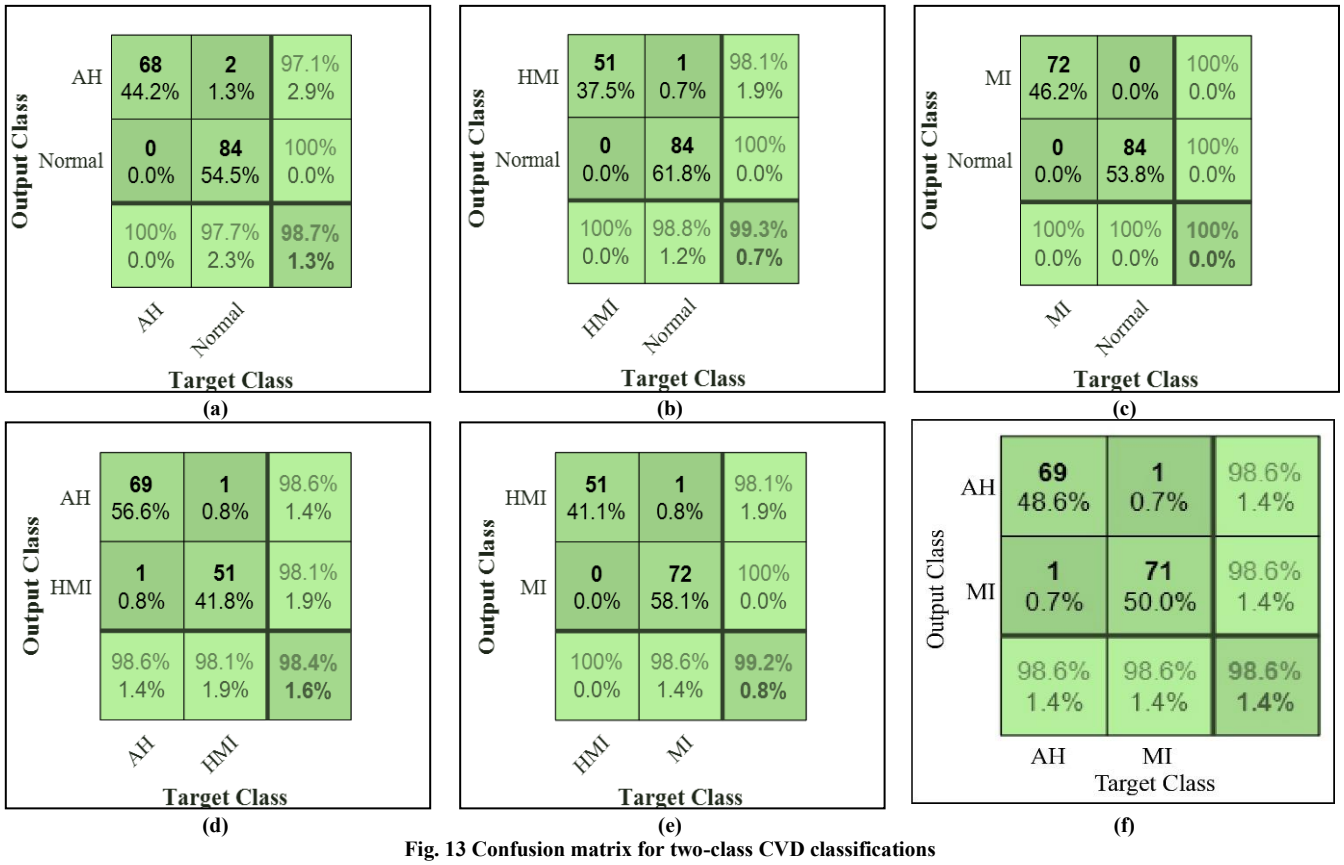

Fig. 13 Confusion matrix for two-class CVD classifications

4.4. Effect of Block Size on CVD Detection (4-Class CVD Detection)

A histogram can be created by considering local areas of the ECG MLTP. The feature representation can be improved by increasing the number of blocks. Due to the redundancy of the features, the feature size increases when N equals four, resulting in fewer results being obtained.

As a result, the MLTP with R = 3 and N = 4 is considered in this study for the DLTWFD.

Table 4. Effect of different block sizes of MLTP on DLTWFD

Algorithm	Radius	Number of Blocks (N)	Recall	Precision	F1-score	Accuracy
DLTWFD (2D-DCNN + 1D-DCNN)	R=1	N=1	87.37	86.86	87.11	87.05
		N=2	88.46	87.74	88.10	88.13
		N=3	89.52	88.80	89.16	89.21
		N=4	90.12	89.59	89.85	89.93
		N=5	89.82	89.19	89.50	89.57
	R=2	N=1	90.61	89.82	90.22	90.22
		N=2	90.96	90.18	90.57	90.58
		N=3	91.32	90.53	90.92	90.94
		N=4	94.79	94.53	94.66	94.58
		N=5	93.35	92.97	93.16	93.14
	R=3	N=1	96.19	96.15	96.17	96.36
		N=2	96.70	96.52	96.61	96.73
		N=3	97.04	97.01	97.03	97.09
		N=4	**98.20**	**98.10**	**98.05**	**98.20**
		N=5	97.40	97.31	97.35	97.46
	R=4	N=1	96.70	96.52	96.61	96.74
		N=2	96.76	96.41	96.58	96.74
		N=3	97.04	96.86	96.95	97.09
		N=4	97.35	97.35	97.35	97.46
		N=5	96.06	95.73	95.90	96.01
	R=5	N=1	91.32	90.53	90.92	90.94
		N=2	92.32	91.72	92.02	92.03
		N=3	95.67	95.57	95.62	95.65
		N=4	96.34	96.27	96.31	96.36
		N=5	95.37	95.22	95.29	95.29

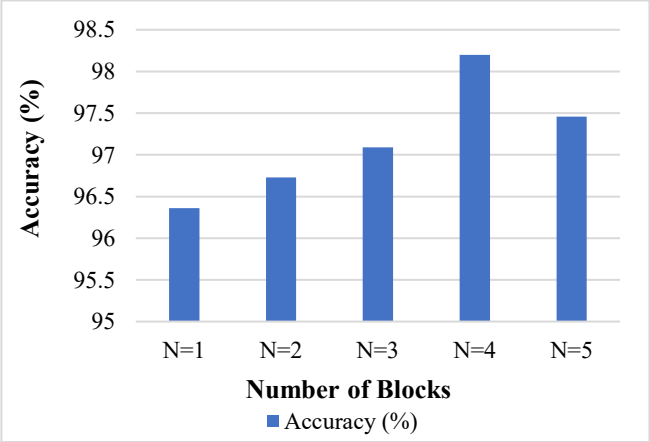

Fig. 14 Accuracy for different block sizes

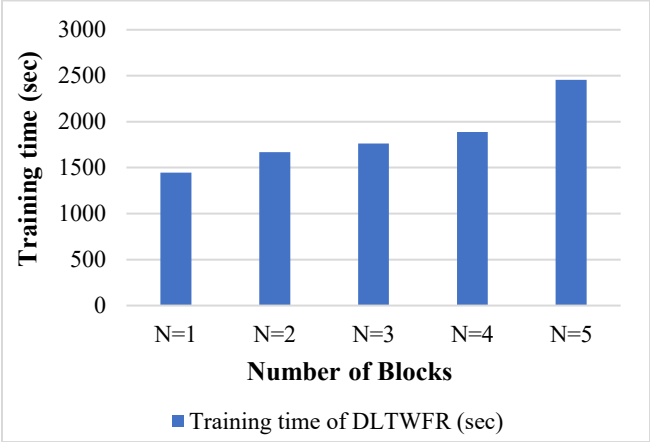

Fig. 15 Training time of DLTWFD (sec) for different blocks

4.5. Training Time Analysis

The amount of time required for training the DLTWFD for R = 3 is shown in Figure 14-16, respectively, for each of the distinct blocks. Furthermore, it has been discovered that the DLTWFD provides optimal training and testing times of 1889 seconds and 1.23 seconds, respectively, for the N=4 value. This results in an exceptional level of accuracy for diagnosing four different types of CVD. With a value of N

equal to five, MLTP offers 12800 histogram features and significantly increases the trainable parameters of the 1D-DCNN. This results in an increase in the computational complexity of the DLTWFD.

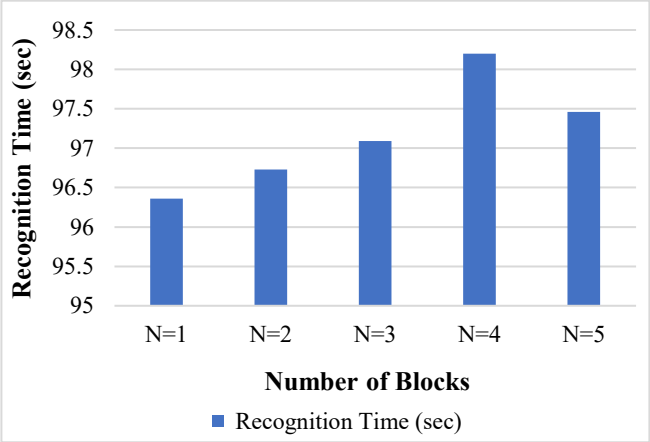

Fig. 16 Recognition time of DLTWFD (sec) for different blocks

4.6. Comparisons with Previous Techniques

We compare the findings of the DLTWFD with those of established approaches that consider ECG images for CVD identification, as shown in Table 5, based on their accuracy. Deep learning models, such as MobileNet V2 and VGG16, were examined by Mhamdi et al. [38] to develop an ECG-based system for CVD diagnosis. The performance of MobileNet V2 was somewhat lower than that of VGG16, which reached an accuracy of 91% and an F1-score of 0.905. MobileNet V2 achieved an accuracy of 95%, while VGG16 earned an F1-score of 0.942. Based on these findings, it can be concluded that deep learning models are successful; however, the complexity of the framework somewhat constrains their performance.

The research conducted by Bhangale and colleagues [39] focused on conventional machine learning methods, including Naïve Bayes, Linear Support Vector Machines (SVM), K-Nearest Neighbors (KNN), and Random Forest. Random Forest achieved the highest accuracy among them, with a score of 96.25%, demonstrating its resilience in feature-based categorization. Additionally, the Linear Support Vector Machine (SVM) demonstrated exceptional performance, achieving an accuracy rate of 95.25%. On the other hand, KNN and Naïve Bayes demonstrated a lesser level of performance, with 83.75% and 70.5%, respectively. In contrast, the Deep Learning with Temporal Wavelet Feature Representation (DLTWFD) technique, which was suggested, achieved an accuracy of 98.20%, significantly outperforming the previous methodologies.

This represents an improvement of 3.95% compared to MobileNet V2, an increase of 7.9% compared to VGG16, and a 2.03% improvement over Random Forest, which was the conventional model that performed the best. As an additional point of interest, the suggested strategy achieved a higher F1-score (98.05), indicating improved overall classification consistency.

Table 5. Comparison of DLTWFD with traditional CVD detection schemes

Authors	Methods	Accuracy (%)	Recall	Precision	F1-score
Mhamdi et al. [38]	MobileNet V2	95	94	97.5	94.2
Mhamdi et al. [38]	VGG16	91	90.5	91.2	90.5
Bhangale et al. [39]	Naïve bayes	70.5	71	71.25	70.75
	Linear SVM	95.25	94.25	95.5	94.25
	KNN	83.75	84.25	84.25	83.5
	Random Forest	96.25	96.25	96.25	96.25
Proposed method	DLTWFD	**98.20**	**98.20**	**98.10**	**98.05**

By integrating the hierarchical, unique characteristics and complex patterns derived from the raw ECG images with the distinctive texture and shape features generated from MLTP, HOG, and morphological features, the proposed DLTWFD can provide a more accurate portrayal of the ECG for the identification of CVD. To provide a greater connection and correlation between the local and global patterns of the ECG, the innovative MLTP facilitates the detection of both fine and coarse alterations in the ECG pattern. By including irregularities in the form of the ECG that are caused by CVDs, the HOG and morphological aspects help to enhance the individuality of the findings. Both the two-class and the four-class classifications provide encouraging findings and demonstrate a high level of classification accuracy. On the other hand, the system's usefulness can be limited by the issue of class imbalance and the small size of the initial dataset. Due to the availability of 2D-DCNN and 1D-DCNN in two arms, the manual parameter adjustment of the DLTWFD presents a degree of difficulty.

5. Conclusion and Future Scopes

Advanced diagnostic methods are required to diagnose cardiovascular disease in a timely and reliable manner, since it continues to be a significant worry for the health of people all over the world.

This research presents a framework for DLTWFD that utilizes both two-dimensional and one-dimensional DCNNs to enhance the identification of CVD using ECG images. By integrating raw ECG image analysis with 2-D DCNN and

feature extraction through 1-D DCNN, using MLTP and HOG features, a comprehensive understanding of local and global alterations in ECG patterns caused by CVD is provided. The suggested DLTWFD enhances feature distinctiveness, resulting in improved classification performance. This is accomplished by efficiently merging deep properties from raw ECG pictures with texture and shape features.

The fact that this strategy achieved an accuracy of 98.20%, recall of 98.20%, precision of 98.10%, and F1-score of 98.05% demonstrates that it is more successful than the approaches currently considered state-of-the-art. Refining the model, improving its computational efficiency, and investigating its potential applications in clinical settings will be the primary focus of future research.

References

[1] Gaziano T et al., *Cardiovascular Diseases*, Disease Control Priorities in Developing Countries, 2nd ed., 2006. [Google Scholar] [Publisher Link]

[2] Connie W. Tsao et al., "Heart Disease and Stroke Statistics-2022 Update: A Report from the American Heart Association," *Circulation*, vol. 145, no. 8, pp. e153-e639, 2022. [CrossRef] [Google Scholar] [Publisher Link]

[3] Connie W. Tsao et al., "Heart Disease and Stroke Statistics-2023 Update: A Report from the American Heart Association," *Circulation*, vol. 147, no. 8, pp. e93-e621, 2023. [CrossRef] [Google Scholar] [Publisher Link]

[4] Md Manjurul Ahsan, and Zahed Siddique, "Machine Learning-Based Heart Disease Diagnosis: A Systematic Literature Review," *Artificial Intelligence in Medicine*, vol. 128, pp. 1-23, 2022. [CrossRef] [Google Scholar] [Publisher Link]

[5] Jahmunah, Vicnesh et al., "Computer-Aided Diagnosis of Congestive Heart Failure Using ECG Signals-A Review," *Physica Medica*, vol. 62, pp. 95-104, 2019. [CrossRef] [Google Scholar] [Publisher Link]

[6] Ali Haider Khan, Muzammil Hussain, and Muhammad Kamran Malik, "Cardiac Disorder Classification by Electrocardiogram Sensing Using Deep Neural Network," *Complexity*, vol. 2021, no. 1, pp. 1-8, 2021. [CrossRef] [Google Scholar] [Publisher Link]

[7] Zachi I. Attia et al., "Application of Artificial Intelligence to the Electrocardiogram," *European Heart Journal*, vol. 42, no. 46, pp. 4717-4730, 2021. [CrossRef] [Google Scholar] [Publisher Link]

[8] Yehualashet Megersa Ayano et al., "Interpretable Machine Learning Techniques in ECG-Based Heart Disease Classification: A Systematic Review," *Diagnostics*, vol. 13, no. 1, pp. 1-37, 2022. [CrossRef] [Google Scholar] [Publisher Link]

[9] Santanu Kumar Sahoo, et al., "Machine Learning Approach to Detect Cardiac Arrhythmias in ECG Signals: A Survey," *IRBM*, vol. 41, no. 4, pp. 185-194, 2020. [CrossRef] [Google Scholar] [Publisher Link]

[10] Atiaf Ayal Rawi, Murtada Kalafalla Albashir, and Awadallah Mohammed Ahmed. "Classification and Detection of ECG Arrhythmia and Myocardial Infarction Using Deep Learning: A Review," *Webology*, vol. 19, no. 1, pp. 1151-1170, 2022. [CrossRef] [Google Scholar] [Publisher Link]

[11] Hongzu Li, and Pierre Boulanger, "A Survey of Heart Anomaly Detection Using Ambulatory Electrocardiogram (ECG)," *Sensors*, vol. 20, no. 5, pp. 1-33, 2020. [CrossRef] [Google Scholar] [Publisher Link]

[12] Carlos Martin-Isla et al., "Image-Based Cardiac Diagnosis with Machine Learning: A Review," *Frontiers in Cardiovascular Medicine*, vol. 7, pp. 1-19, 2020. [CrossRef] [Google Scholar] [Publisher Link]

[13] Lakshmi Prasad Koyi, Tejaswi Borra, and G. Lakshmi Vara Prasad, "A Research Survey on State of the art Heart Disease Prediction Systems," *2021 International Conference on Artificial Intelligence and Smart Systems (ICAIS)*, Coimbatore, India, pp. 799-806, 2021. [CrossRef] [Google Scholar] [Publisher Link]

[14] Xinwen Liu et al., "Deep Learning in ECG Diagnosis: A Review," *Knowledge-Based Systems*, vol. 227, 2021. [CrossRef] [Google Scholar] [Publisher Link]

[15] Shenda Hong et al., "Opportunities and Challenges of Deep Learning Methods for Electrocardiogram Data: A Systematic Review," *Computers in Biology and Medicine*, vol. 122, pp. 1-16, 2022. [CrossRef] [Google Scholar] [Publisher Link]

[16] Steve S. Ryan, Understanding the EKG Signal, Atrial Fibrillation: Resources for Patients, 2020. [Online] Available: https://a-fib.com/treatments-for-atrial-fibrillation/diagnostic-tests-2/the-ekg-signal

[17] Yasar Sattar, and Lovely Chhabra, *Electrocardiogram*, StatPearls Publishing, 2023. [Google Scholar] [Publisher Link]

[18] Ana Mincholé, and Blanca Rodriguez, "Artificial Intelligence for the Electrocardiogram," *Nature Medicine*, vol. 25, no. 1, pp. 22-23, 2019. [CrossRef] [Google Scholar] [Publisher Link]

[19] Donna Giri et al., "Automated Diagnosis of Coronary Artery Disease Affected Patients using LDA, PCA, ICA, and Discrete Wavelet Transform," *Knowledge-Based Systems*, vol. 37, pp. 274-282, 2013. [CrossRef] [Google Scholar] [Publisher Link]

[20] Shivnarayan Patidar, Ram Bilas Pachori, and U. Rajendra Acharya, "Automated Diagnosis of Coronary Artery Disease Using Tunable-Q Wavelet Transform Applied on Heart Rate Signals," *Knowledge-Based Systems*, vol. 82, pp. 1-10, 2015. [CrossRef] [Google Scholar] [Publisher Link]

[21] Mohit Kumar, Ram Bilas Pachori, and U. Rajendra Acharya, "An Efficient Automated Technique for CAD Diagnosis Using Flexible Analytic Wavelet Transform and Entropy Features Extracted from HRV Signals," *Expert Systems with Applications*, vol. 63, pp. 165-172, 2016. [CrossRef] [Google Scholar] [Publisher Link]

[22] Surabhi Sood et al., "Application of Empirical Mode Decomposition-Based Features for Analysis of Normal and Cad Heart Rate Signals," *Journal of Mechanics in Medicine and Biology*, vol. 16, no. 1, pp. 1-20, 2016. [CrossRef] [Google Scholar] [Publisher Link]

[23] Roohallah Alizadehsani et al., "Coronary Artery Disease Detection Using Computational Intelligence Methods," *Knowledge-Based Systems*, vol. 109, pp. 187-197, 2016. [CrossRef] [Google Scholar] [Publisher Link]

[24] Zeinab Arabasadi et al., "Computer-Aided Decision Making for Heart Disease Detection Using a Hybrid Neural Network-Genetic Algorithm," *Computer Methods and Programs in Biomedicine*, vol. 141, pp. 19-26, 2017. [CrossRef] [Google Scholar] [Publisher Link]

[25] Tahmida Tabassum, and Monira Islam, "An Approach of Cardiac Disease Prediction by Analyzing ECG Signal," *2016 3rd International Conference on Electrical Engineering and Information Communication Technology (ICEEICT)*, Dhaka, Bangladesh, pp. 1-5, 2016. [CrossRef] [Google Scholar] [Publisher Link]

[26] Aditi Gavhane et al., "Prediction of Heart Disease Using Machine Learning," *2018 Second International Conference on Electronics, Communication and Aerospace Technology (ICECA)*, Coimbatore, India, pp. 1275-1278, 2018. [CrossRef] [Google Scholar] [Publisher Link]

[27] Senthilkumar Mohan, Chandrasegar Thirumalai, and Gautam Srivastava, "Effective Heart Disease Prediction Using Hybrid Machine Learning Techniques," *IEEE Access*, vol. 7, pp. 81542-81554, 2019. [CrossRef] [Google Scholar] [Publisher Link]

[28] Vineet Sharma, Akhtar Rasool, and Gaurav Hajela, "Prediction of Heart Disease Using DNN," *2020 Second International Conference on Inventive Research in Computing Applications (ICIRCA)*, Coimbatore, India, pp. 554-562, 2020. [CrossRef] [Google Scholar] [Publisher Link]

[29] Jian Ping Li et al., "Heart Disease Identification Method Using Machine Learning Classification in E-Healthcare," *IEEE Access*, vol. 8, pp. 107562-107582, 2020. [CrossRef] [Google Scholar] [Publisher Link]

[30] K. Prajwal et al., "Cardiovascular Disease Prediction Using Machine Learning," *2022 International Conference on Innovative Trends in Information Technology (ICITIIT)*, Kottayam, India, pp. 1-6, 2022. [CrossRef] [Google Scholar] [Publisher Link]

[31] Yan Fang et al., "Electrocardiogram Signal Classification in the Diagnosis of Heart Disease Based on RBF Neural Network," *Computational and Mathematical Methods in Medicine*, vol. 2022, no. 1, pp. 1-9, 2022. [CrossRef] [Google Scholar] [Publisher Link]

[32] Niloy Biswas et al., "Machine Learning-Based Model to Predict Heart Disease in Early Stage Employing Different Feature Selection Techniques," *BioMed Research International*, vol. 2023, no. 1, pp. 1-15, 2023. [CrossRef] [Google Scholar] [Publisher Link]

[33] Ali Haider Khan, and Muzammil Hussain, "ECG Images Dataset of Cardiac Patients," *Mendeley Data*, vol. 2, 2021. [CrossRef] [Publisher Link]

[34] Kishor B. Bhangale, and K. Mohanaprasad, "Content Based Image Retrieval Using Collaborative Color, Texture and Shape Features," *International Journal of Innovative Technology and Exploring Engineering (IJITEE)*, vol. 9, no. 3, pp. 1466-1469, 2020. [CrossRef] [Google Scholar] [Publisher Link]

[35] Y.G. Naresh, and H.S. Nagendraswamy, "Classification of Medicinal Plants: An Approach Using Modified LBP with Symbolic Representation," *Neurocomputing*, vol. 173, pp. 1789-1797, 2016. [CrossRef] [Google Scholar] [Publisher Link]

[36] Li Liu et al., "Extended Local Binary Patterns for Texture Classification," *Image and Vision Computing*, vol. 30, no. 2, pp. 86-99, 2012. [CrossRef] [Google Scholar] [Publisher Link]

[37] Xiaoyang Tan, and Bill Triggs, "Enhanced Local Texture Feature Sets for Face Recognition Under Difficult Lighting Conditions," *IEEE Transactions on Image Processing*, vol. 19, no. 6, pp. 1635-1650, 2010. [CrossRef] [Google Scholar] [Publisher Link]

[38] Lotfi Mhamdi et al., "Artificial Intelligence for Cardiac Disease Diagnosis and Prediction Using ECG Images on Embedded Systems," *Biomedicines*, vol. 10, no. 8, pp. 1-16, 2022. [CrossRef] [Google Scholar] [Publisher Link]

[39] Kishor Bhangale et al., "Machine Learning Based Heart Disease Prediction Using ECG Image," *2024 5th International Conference for Emerging Technology (INCET)*, Belgaum, India, pp. 1-9, 2024. [CrossRef] [Google Scholar] [Publisher Link]